

# RX J0719.2+6557: A new eclipsing polar

G.H. Tovmassian<sup>1</sup>, J. Greiner<sup>2\*</sup>, F.-J. Zickgraf<sup>2\*\*</sup>, P. Kroll<sup>3</sup>, J. Krautter<sup>4</sup>, I. Thiering<sup>4</sup>, S.V. Zharykov<sup>5</sup>, and A. Serrano<sup>6</sup>

<sup>1</sup> Observatorio Astronomico Nacional, Instituto de Astronomía, UNAM, AP 877, 22860, Ensenada, B.C., México

<sup>2</sup> Max-Planck-Institut für extraterrestrische Physik, 85740 Garching, Germany

<sup>3</sup> Sternwarte Sonneberg, 96515 Sonneberg, Germany

<sup>4</sup> Landessternwarte Königstuhl, 69117 Heidelberg, Germany

<sup>5</sup> Special Astronomical Observatory, 357147 Nizhnij Arkhyz, Russia

<sup>6</sup> Instituto Nacional de Astrofísica Óptica y Electrónica, AP 51 y 216, Puebla, Pue., Mexico

Received 31 December 1996 / Accepted 1 August 1997

**Abstract.** A new magnetic cataclysmic variable is identified as the counterpart of the X-ray source RX J0719.2+6557 which has been discovered during the ROSAT all-sky survey. Optical spectroscopy of the  $\approx 17^m$  object revealed a pattern of Balmer and strong He II emission lines which are characteristic for cataclysmic variables. The emission lines show radial velocity variations with a period of 98.2 min with no significant phase shifts among them. This coincides with the period of deep eclipses (up to 4 mag) in the photometric light curve of the system. The phase of the eclipse relative to the spectroscopic phase, and its structure indicates that the dominant source of emission is located on the stream of accreting matter, which is eclipsed by the secondary companion. The emission lines bear evidence of a weaker component, most probably the contribution from the heated side of the secondary star. These features define this object as a probable polar in a high state in which the secondary is irradiated by the X-rays originating from magnetically driven accretion onto the white dwarf. The near-infrared spectroscopy revealed some unusual, strong emission features at 8200 Å and 8660 Å possibly originating on the heated side of the secondary.

**Key words:** stars: cataclysmic variables – accretion – stars: individual: RX J0719.2+6557 – binaries: eclipsing – X-rays: stars

## 1. Introduction

Within a program devoted to the optical identification of a complete sample of northern ROSAT all-sky survey (RASS) X-ray sources we identified a new cataclysmic variable. The identification project is a collaboration of the Max-Planck-Institut für extraterrestrische Physik, Garching, Germany, with the Landessternwarte Heidelberg (LSW), Germany, and the Instituto Nacional de Astrofísica, Óptica y Electrónica (INAOE), Puebla, Tlaxiaco, Mexico. A detailed description of the project is given by Zickgraf et al. (1997).

For the study areas the individual scan strips of the all-sky survey were merged to produce a final data base comprising about 1600 X-ray sources with a detection likelihood larger than 10 corresponding to X-ray detection limits of  $\sim 0.003$  ctss<sup>-1</sup> in area near the North Ecliptic Pole and  $\sim 0.01$  ctss<sup>-1</sup> in all other areas. Since October 1991 nearly 800 X-ray sources have been observed within the identification program. Here we report the identification and detailed follow-up observations of the ROSAT all-sky survey X-ray source RX J0719.2+6557 (= 1RXS J071913.4+655734), first results of which have been reported already earlier (Tovmassian et al. 1997).

Cataclysmic variables (CVs) are close binary systems, in which a compact white dwarf (WD) primary accretes matter from a Roche-lobe filling late-type main-sequence secondary component. Polars are a subclass of cataclysmic variables where the magnetic field of the white dwarf is strong enough to channel the accretion along the magnetic field lines, thus preventing the formation of an accretion disc and synchronizing the rotation of the white dwarf with the orbital period (Warner 1995). A hot spot (or accretion spot) which is formed as a result of a shock of accreting matter before hitting the white dwarf gives rise to hard X-ray radiation (often described with a bremsstrahlung model).

---

Send offprint requests to: G.H. Tovmassian, gag@bufadora.astrosen.unam.mx

\* Present address: Astrophysical Institute Potsdam, An der Sternwarte 16, 14482 Potsdam, Germany

\*\* Present address: Observatoire de Strasbourg, 11 rue de l'Université, F-67000 Strasbourg, France

**Table 1.** Log of Optical Observations

Date	JD	Telescope + Equip.	Filter Wavelength	Duration (min.)	Exposure (sec.)	Site
1996 April 07	2450180	2.1m, B&Ch sp.	3600–5400	60	1200	SPM
1996 April 08	2450181	2.1m, B&Ch sp.	3600–5400	180	600	SPM
1996 April 09	2450182	2.1m, B&Ch sp.	6000–9000	80	600	SPM
1996 April 10	2450183	2.1m, B&Ch sp.	3600–5400	80	1200	SPM
1996 April 15	2450189	0.6m, CCD	B	200	60,120	Sonneberg
1996 April 16	2450190	0.6m, CCD	B	180	120	Sonneberg
1996 April 17	2450191	0.6m, CCD	B	70	90	Sonneberg
1996 August 8/9	2450304	0.6m, CCD	R	100	120	Sonneberg
1996 September 3/4	2450330	0.6m, CCD	R	110	90	Sonneberg
1996 October 08	2450366	1.0m, CCD	B	135	300	Zelenchuk
1996 December 04	2450422	0.6m, CCD	B, R	220	90,120	Sonneberg
1996 December 10	2450428	0.6m, CCD	B, R	380	90	Sonneberg

## 2. X-ray observations

The location of RX J0719.2+6557 was scanned in the RASS during September 22–24, 1990 for a total exposure time of 570 sec. RX J0719.2+6557 is found as a source with a total of 66 photons, which corresponds to a vignetting corrected countrate of 0.16 cts/s in the ROSAT PSPC. No strong variability in the X-ray intensity is seen at this statistics, in particular also no orbital variations. The spectrum as derived from these 66 photons is rather hard, extending up to 2.4 keV (the upper bound of the PSPC). The standard hardness ratio (HR1 is the normalized count difference  $(N_{52-201} - N_{11-41}) / (N_{11-41} + N_{52-201})$ , where  $N_{a-b}$  denotes the number of counts in the PSPC between channel a and channel b, and HR2 is similarly defined as  $(N_{91-200} - N_{50-90}) / N_{50-200}$  with the count number divided by hundred corresponding roughly to the energy in keV) values are  $HR1 = 0.48 \pm 0.12$  and  $HR2 = 0.50 \pm 0.12$ . A thermal bremsstrahlung model gives a reasonable fit for a rather wide range of temperatures (2–15 keV). For a fixed temperature of  $kT=10$  keV the best fit absorbing column is  $1.6 \times 10^{20} \text{ cm}^{-2}$ , and the unabsorbed flux is  $2 \times 10^{-12} \text{ erg/cm}^2/\text{s}$  in the 0.1–2.4 keV range. This is a lower limit because any, even very weak, soft component as usually found in polars would require a higher absorbing column to be compatible with the observed X-ray spectrum. RX J0719.2+6557 has not been covered by any (serendipitous) ROSAT pointing until the time of this writing, so that the X-ray parameters cannot be improved further.

Given the rather low absorbing column (which varies by only 30% for models with different temperature) as compared to the total galactic column in the direction of RX J0719.2+6557 of  $4.6 \times 10^{20} \text{ cm}^{-2}$  (Dickey & Lockman 1990) the distance of RX J0719.2+6557 is possibly only about 100 pc. Again, this is a lower limit in the sense that any (expected, but due to statistics and background contamination not detectable) soft blackbody-like component would result in an increase of the absorbing column

and thus an increased distance. At this distance the (lower limit of the) phase-averaged, unabsorbed X-ray luminosity is  $2.5 \times 10^{30} (D/100\text{pc})^2 \text{ erg/s}$  in the 0.1–2.4 keV range.

## 3. Results of optical observations

### 3.1. Observational details

The original identification observations were carried out at the 2.15 m telescope of the Guillermo Haro Observatory which is operated by INAOE and is located near Cananea, Sonora, Mexico. For the purpose of the identification project the LSW has constructed an efficient faint object spectrograph (*LFOSC*). It allows to carry out direct CCD imaging, filter photometry, and, in particular, multi-object spectroscopy by using interchangeable hole masks with circular holes in the focal plane of the telescope (Zickgraf et al. 1997). Grisms follow in the parallel beam section of the focal reducer. The hole masks are produced from the CCD frames of the direct images with a computer controlled drilling device. Two grisms are available, giving a resolution of 13 Å and 18 Å, respectively. First direct imaging was carried out on January 24, 1993, revealing the presence of four candidates brighter for the optical counterpart than  $R = 23^m$  in the error circle of RX J0719.2+6557. Multi-object spectroscopy with a resolution of 18 Å of the candidates was performed in January 25, 1993. Inspection of the spectra showed the optically brightest candidate to be an emission line object with spectral characteristics typical for cataclysmic variables.

Further detailed study of the emission line object, and its final identification as a new polar, was performed at the 2.1 m telescope of the Observatorio Astronómico Nacional (OAN) de San Pedro Mártir, Mexico in early April 1996. The Boller & Chivens spectrograph was used to obtain spectra of the object. Two wavelength ranges were observed. A 600 l/mm grating was used to obtain spectra in the  $\lambda\lambda 3600-5400 \text{ Å}$  range. In combination with a  $2''$  slit a 4 Å FWHM resolution is reached. The  $\lambda\lambda 6000-9000 \text{ Å}$  range was covered with 6 Å resolution using a 400 l/mm

**Table 2.** Observed minima (eclipses) in the B band

Date	Min. (HJD)	E	(O–C)
1996 April 15	2450189.46324	0	–0.00002
1996 April 16	2450190.35017	13	+0.00023
1996 April 16	2450190.41861	14	+0.00047
1996 April 17	2450191.44190	29	+0.00066
1996 October 08	2450366.52778	2596	–0.00083
1996 December 04	2450422.39000	3415	–0.00014
1996 December 04	2450422.45704	3416	–0.00131
1996 December 10	2450428.52597	3505	–0.00282
1996 December 11	2450428.59522	3506	–0.00178
1996 December 11	2450428.66326	3507	–0.00195

grating. Exposure times of 600 sec. were chosen as a compromise between high temporal resolution in order to derive the orbital period of the system and well exposed spectra. The seeing during the first three nights was about  $1''.5$ , while in the last night it was  $2''.3$ – $2''.5$ , and the air was contaminated by dust brought up by storm. In total, we obtained 23 spectra in the blue part, distributed over three nights. Additional 8 spectra were obtained in the red side of the spectrum during one night. The standard stars Feige 34 and HZ 44 were observed each night for flux calibration. Comparison spectra were taken every 20 minutes. They were used for wavelength calibration precise up to  $0.3\text{\AA}$  and actual dispersion solutions were assigned to the object spectra based upon the julian date. The spectra were reduced using standard routines in the IRAF package. Spectrum extraction was performed according to the optimal extraction method as described by Horne (1986).

Extensiv optical photometry was first performed on three nights in 1996 April (15/16 and 16/17 and 17/18, some ten days after the spectroscopic observations) at the Sonneberg Observatory 600/1800 mm reflector, equipped with a  $385\times 578$  pixel EEV CCD. Exposure times were 60 to 120 sec., and a Johnson B filter was used. Further photometry was acquired in August and September 1996 in the R band, and in December 1996 with alternating exposures using Johnson B and R filters, respectively.

One photometric run was also obtained at the Special Astrophysical Observatory (Zelenchuk) 1 m telescope over more than two hours with 5 min. exposures each in the B band. A log of all optical observations is summarized in Tab. 1.

### 3.2. Identification and position

The sequence of spectra of the emission line object taken with the 2.1 m telescope shows strong emission lines of the Balmer series, He I and He II on top of a blue continuum. Though no polarimetric measurements were performed, the relative line strengths are characteristic for magnetic cataclysmic variables (CVs).

We measure the position of the optical counterpart of RX J0719.2+6557 as (equinox 2000.0) R.A. =  $07^{\text{h}}19^{\text{m}}14^{\text{s}}.0$ ,

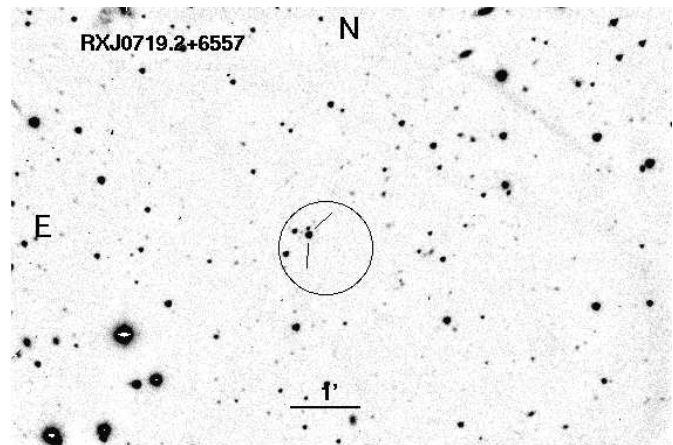


**Fig. 1.** R band image of the field around the X-ray source RX J0719.2+6557 (centroid position with a  $40''$  ( $3\sigma$ ) error circle). The cataclysmic variable is marked by two dashes.

Dec. =  $65^{\circ}57'48''(\pm 1'')$ . Fig. 1 shows a finding chart with the magnetic cataclysmic variable marked.

### 3.3. Eclipse lightcurve

Optical photometry clearly shows an eclipsing light curve (Fig. 2). The eclipse FWHM is about 5 min, and the eclipse depth is strongly variable reaching a maximum amplitude of nearly 4 mag in the blue band. The short ingress and egress durations suggest that the emission region is compact, and we associate it with the hot spot on the accretion stream toward the white dwarf. Our temporal resolution (typically 2 min.) does not allow to investigate possible persistent structures in the eclipse ingress or egress. The large amplitude of the eclipses implies that this compact emission region is by far the dominant light source in this binary system.

The eclipses are regular and stable over months. The eclipse moments were measured as a center of a gaussian fit to the eclipse profile in the B band. We searched for the most probable period using a least squares method applied to the timings of the eclipse minima given in Tab. 2. For a fixed  $T_0 = 2450189.46324$  we calculated the phasing of all timings for a range of trial periods. The inverted sum of the squared (O–C) values resulting from that, is plotted as a function of the trial period in Fig. 3. It shows a prominent peak at  $P = 0.068207 \pm 0.000019$  days, which we adopted as the eclipse period. We derive the following ephemeris:

$$T_{\text{ecl}} = \text{HJD}2450189.46326 + 0^{\text{d}}.068207[19] \times E$$

In the following  $\phi_{\text{orb}}$  refers to this ephemeris.

### 3.4. Orbital modulation

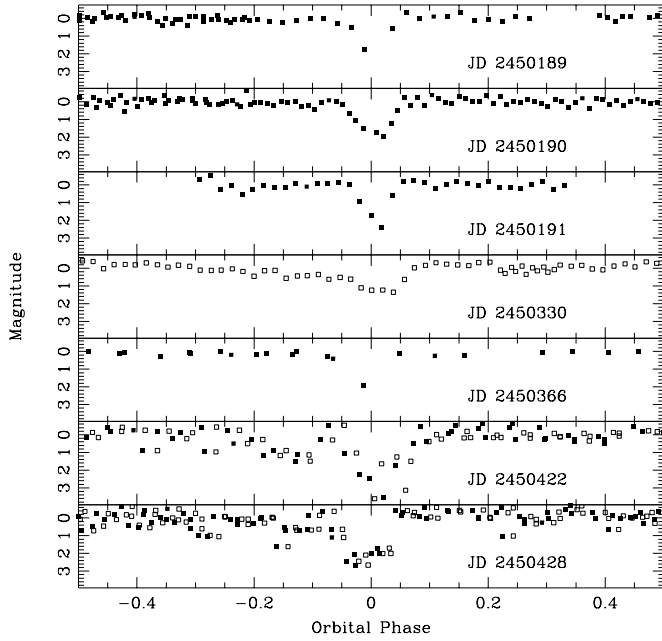


**Fig. 2.** Light curves of RX J0719.2+6557 folded with the orbital period. Filled (open) symbols denote B (R) band measurements. The errors are smaller than the symbol size. Note the varying width of the flux depression before the eclipse as well as the varying eclipse depth.

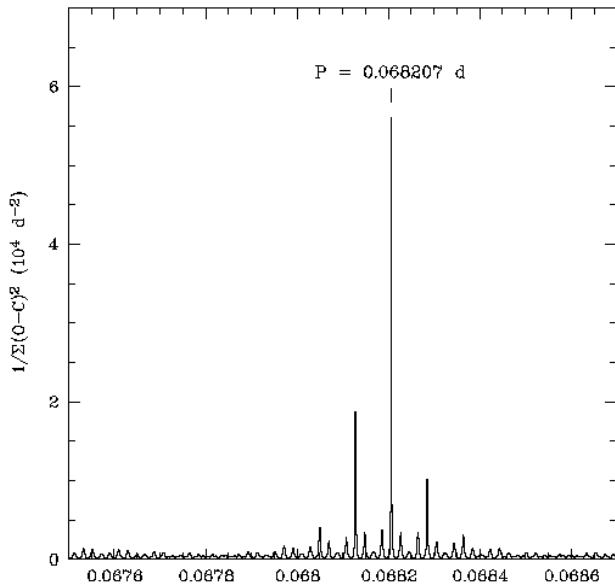


**Fig. 3.** Result of our period analysis (see text). The value given at the y-axis is the inverted sum of the squared (O-C)-values resulting from the eclipse timings observed. The period derived from our linear regression is marked.

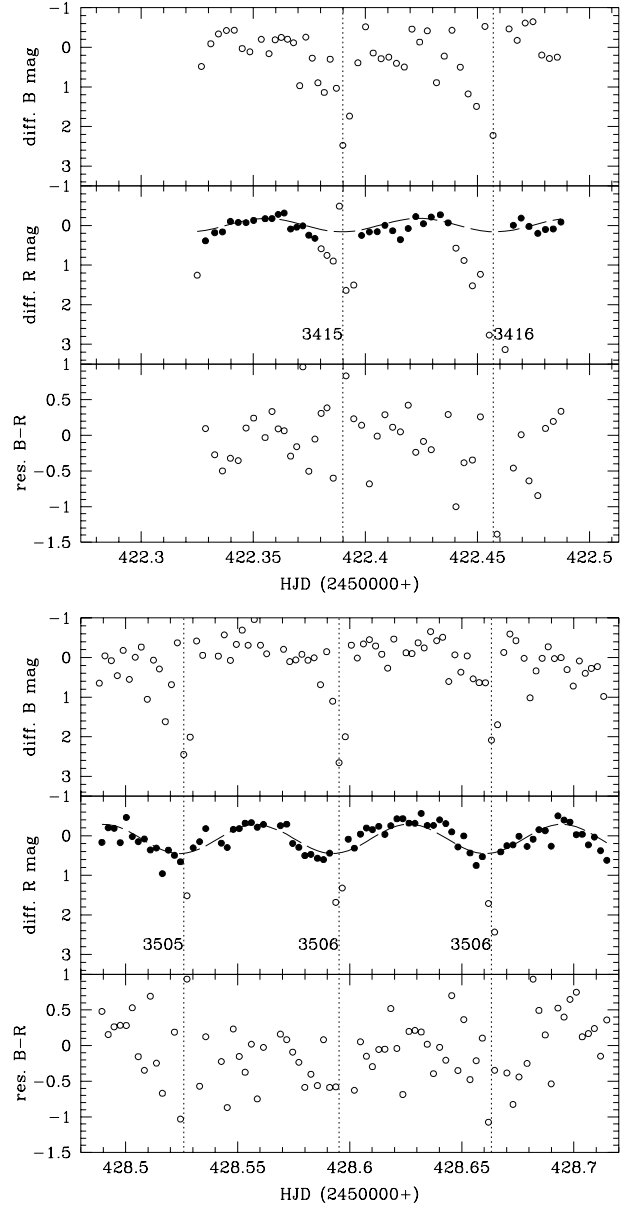


**Fig. 4.** Two sequences of alternating B and R exposures of RX J0719.2+6557 obtained on Dec. 4/5 and Dec. 10/11, respectively. The error of each data point is about the symbol size. The vertical dotted lines mark the times of the mid-eclipse according to the photometric ephemeris, and numbers in the R band panels denote the cycle number (see also Tab. 2). The filled circles in the R band panels were used to fit a sin curve, while open circles (during eclipse) were omitted. The relative colour B-R has been computed by equating the mean between two B measurements with the simultaneous R measurement.

In addition to the eclipse profile, another noteworthy feature of the light curves is the strong modulation seen outside the eclipse. This feature is not strongly persistent, and most prominently seen in the R band (see Fig. 4). Though one would expect the light curve to be more complicated, the R band variations could be successfully fitted by a sinusoid, if we ignore the points within the eclipses (Fig. 4). We think that the R band variations are due to the varying aspect of the X-ray heated side of the secondary although the directionality of optical synchrotron emission is a viable alternative. If we proceed with this interpretation, it is worth to note that the eclipse occurs with a slight delay relative to the secondary inferior conjunction, estimated as a minima on a fitted sin curve. It could be attributed to the fact, that the hot spot actually is located at some height (i.e. on the accretion stream) or that the heated spot on the surface of the secondary is not symmetric. However, the latter is less probable and we will see in the next paragraph that spectroscopic observations also favour the first interpretation.

### 3.5. Spectral and radial velocity variations

Flux-calibrated spectra of RX J0719.2+6557 in both spectral ranges during an eclipse and a phase interval opposite to the eclipse ( $\phi_{orb} \simeq 0.5$ ) are shown in Fig. 5. The spectra are from the nights with the better seeing. Although the exposure times are as long as the full duration of the eclipse and not exactly centered on it, significant variations between the in- and out-of-eclipse spectra are observed, in particular concerning the line strengths.

The mean values of major emission lines and their equivalent widths out of eclipse are presented in Tab. 3. The dependence of these values on orbital phases are presented in Fig. 6. The continuum fluxes mark the eclipse clearly in the lower panel. The Balmer lines show a smaller drop of flux strength relative to He II, while the equivalent width of H $\beta$  exhibits a large increase during eclipse in contrast to He II. This implies that the eclipse affects the continuum and He II more than Balmer lines.

**Table 3.** Flux and Equivalent Width of Emission Lines

Emission Line	Log Flux ( $erg/cm^2/s/\text{\AA}$ )	E.W. ( $\text{\AA}$ )	FWHM ( $\text{\AA}$ )
H $\delta$	$-13.70 \pm 0.10$	$-55 \pm 8$	
H $\gamma$	$-13.65 \pm 0.08$	$-67 \pm 10$	
H $\beta$	$-13.60 \pm 0.08$	$-72 \pm 10$	$20 \pm 2$
H $\alpha$	$-13.50 \pm 0.15$	$-101 \pm 14$	$30 \pm 3$
He I 4471	$-14.12 \pm 0.10$	$-21 \pm 7$	
He II 4686	$-14.10 \pm 0.10$	$-37 \pm 10$	$14 \pm 4$

We used the double Gaussian deconvolution and the diagnostic method suggested by Schneider and Young (1980) and Shafter (1985) to measure radial velocity vari-

ations. Two Gaussians with fixed width and separation are convolved with an emission line. The position of equal intensity Gaussians corresponds to the line center. The width and separation could be changed in order to get use of different parts of line wings. Shafter (1985) describes the technique how to choose the optimal separation. We used a 4  $\text{\AA}$  FWHM gaussians corresponding to our spectral resolution and follow the mentioned diagnostic method to pick up a 10  $\text{\AA}$  half-separation as the best parameter to measure the emission line centers.

The spectroscopic period as derived from the line center variations of H $\beta$  shows maximum peak in the power spectrum at  $0.067916 \pm 0.000576$  days. This coincides within reasonable limits with the 98.2 min. period as derived from the moments of eclipses. The 98.2 min. (0<sup>d</sup>068207) period was therefore adopted as the orbital period of the system. The radial velocity (RV) curves (see Fig. 7) were non-linearly fitted by the following function:

$$V_{em} = \gamma + K_{em} \sin(2\pi\omega + \phi) \quad (1)$$

where  $\omega = t - T_0/P_{orb}$ .

Phase zero ( $T_0$ ) was chosen for H $\beta$ , so that  $\phi = \pi n$ , where n is an integer number. This implies the following ephemeris:

$$\begin{aligned} \text{for H}\beta: \quad & \gamma = -38.4 \text{ km/sec} \\ & T_0 = 2450180.574398 \pm 0.00007 \\ & K_{em} = 245.7 \pm 1.5 \text{ km/sec} \\ \text{for He II: } & \gamma = -42.0 \text{ km/sec} \\ & T_0 = 2450180.57348 \pm 0.00009 \\ & K_{em} = 318.4 \pm 2.3 \text{ km/sec} \end{aligned}$$

According to this, the -/+ crossing of the RV curve occurs at orbital phase  $\phi_{orb} = 0.68$  (for H $\beta$ ). The obtained amplitudes of the radial velocities are significantly higher than one would expect from orbital motion of the WD, but would not be unexpected for emission formed in an accretion stream, where the intrinsic velocities can be quite high.

Although we tried a wide range of gaussian separations, the procedure was incapable to distinguish the presence of components other than measured in the emission lines. However, a careful study of the trailed spectra shows complex structure of emission lines during some phase intervals. In order to reveal the weaker component we fitted H $\beta$  with a single gaussian with the center calculated from Eq. 1 and variable widths. Then we subtracted the fit from the actual line profile. The residuals, in form of trailed spectra, are presented in the right panel of Fig. 7, while on the left panel the original spectra (normalized to the continuum) are displayed with levels of grey allowing the best visualization of the spectroscopic period. The residual spectra bear inside a weak trace of emission shifted in phase to the spectroscopic period. The feature varies in strength and is most prominent at orbital phases  $0.25 > \phi_{orb} > 0.75$  marked on the right panel. We measured the radial velocity variations of this feature and

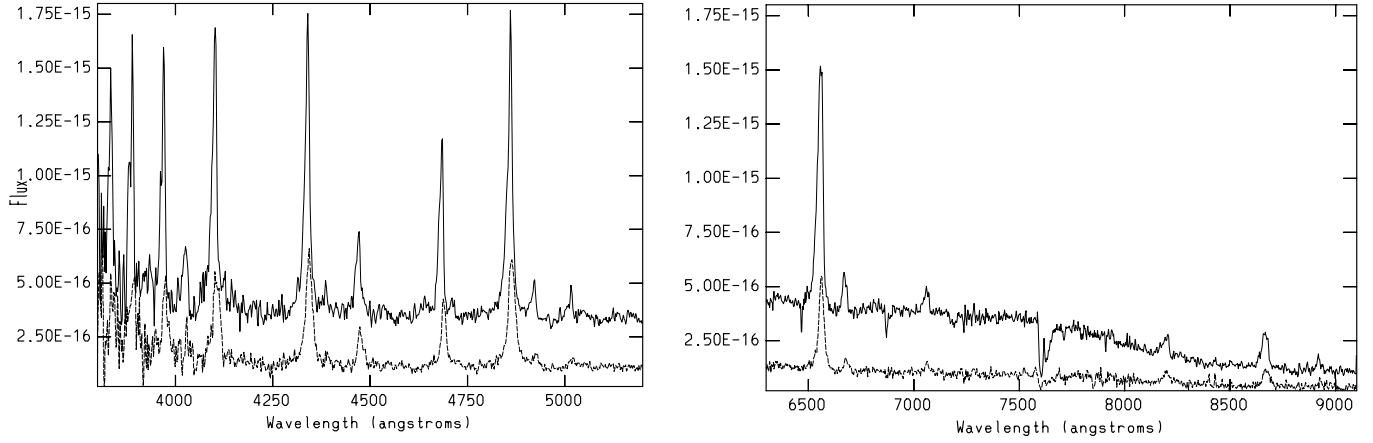


**Fig. 5.** The spectra of RX J0719.2+6557 in the blue (left panel) and red (right). The solid line represents the spectrum out of eclipse, the dashed line is the spectrum during eclipse. The flux unit is in  $\text{erg}/\text{cm}^2/\text{s}/\text{\AA}$ .

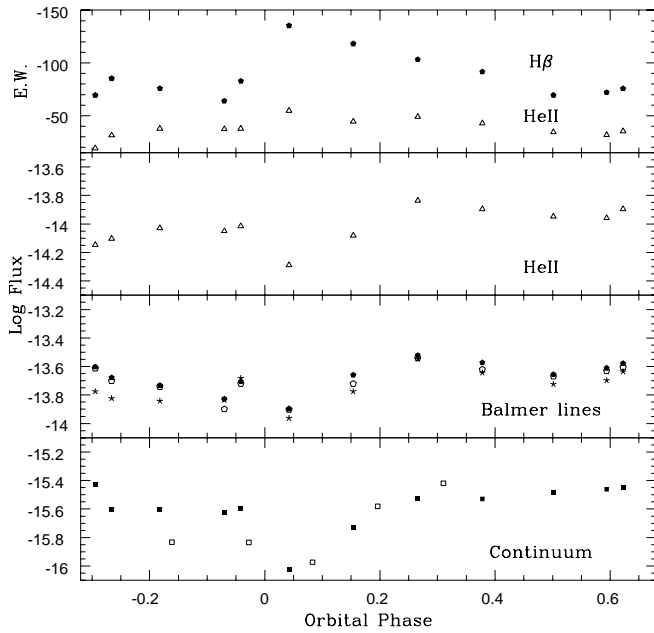


**Fig. 6.** Orbital variation of the continuum fluxes and major lines. The continuum measurements around  $\lambda 4700 \text{ \AA}$  (filled symbols) and  $\lambda 6500 \text{ \AA}$  (open symbols) are shown in the lower panel. The  $\text{H}\beta$  (filled),  $\text{H}\gamma$  (open) and  $\text{H}\delta$  (starlike symbols) fluxes are in the next panel. In the third panel the fluxes of He II are displayed. The top panel shows the variation of the equivalent widths of  $\text{H}\beta$  and He II. Flux units are in  $\text{erg}/\text{cm}^2/\text{s}/\text{\AA}$  and the equivalent width EW in  $\text{\AA}$ . Because of the time resolution of only 7 min. ( $\approx 0.07$  phase units) achieved in the spectroscopic observations the minima do not exactly match the photometric (orbital) eclipse phase.

display these in the lower panel of Fig. 7 (solid circles). Considering its period to be equal to the orbital one, and assigning the bad shape to our inaccuracy of the measurements, we assume that its  $-/+$  crossing occurs at the

eclipse and that it becomes brighter at phases when we are facing the secondary component.

The filtered backprojection method (Marsh & Horne 1988) was applied to the lines of He II and  $\text{H}\beta$  with the orbital (photometric) phase registration adopted above. As we noted above the eclipse probably does not coincide precisely with the conjunction of the stellar components. However, its phase shift is not significant for the figure we obtain by doppler tomography since it gives us a general impression of the system configuration, but no quantitative measurements. The resulting velocity maps (tomograms) are presented in Fig. 8. The spectra of both lines are displayed as trailed gray-scale images on the left. On the maps the secondary is located along the  $+V_Y$  axis and the WD along  $-V_Y$ . It is evident that the He II emission region is compact and concentrated at the expected location of the accretion stream/hot spot. Unlike He II,  $\text{H}\beta$  shows a more diffuse distribution and spreads out to the inner  $L_1$  point.

### 3.6. Geometric Configuration

Given the presence of eclipses, the inclination  $i$  of the orbital plane of the system is  $78^\circ \lesssim i \leq 90^\circ$ . The accretion stream with its hot spot is the main contributor of radiation. It is the hot spot which we see being occulted and it is also the major contributor of the emission lines, producing radial velocity variations responsible for spectroscopic phasing. The other observable component in the emission lines is due to the secondary with the heated surface facing the hot, bright spot. The irradiated part of the secondary produces the single humped light curve in the R band and the weak component of emission lines. The hot spot is located on the accretion stream but it is not yet clear where it is along the stream. The possible locations are: during the ballistic part before the coupling to the WD magnetic field, i.e. when the stream is still inside the orbital plane

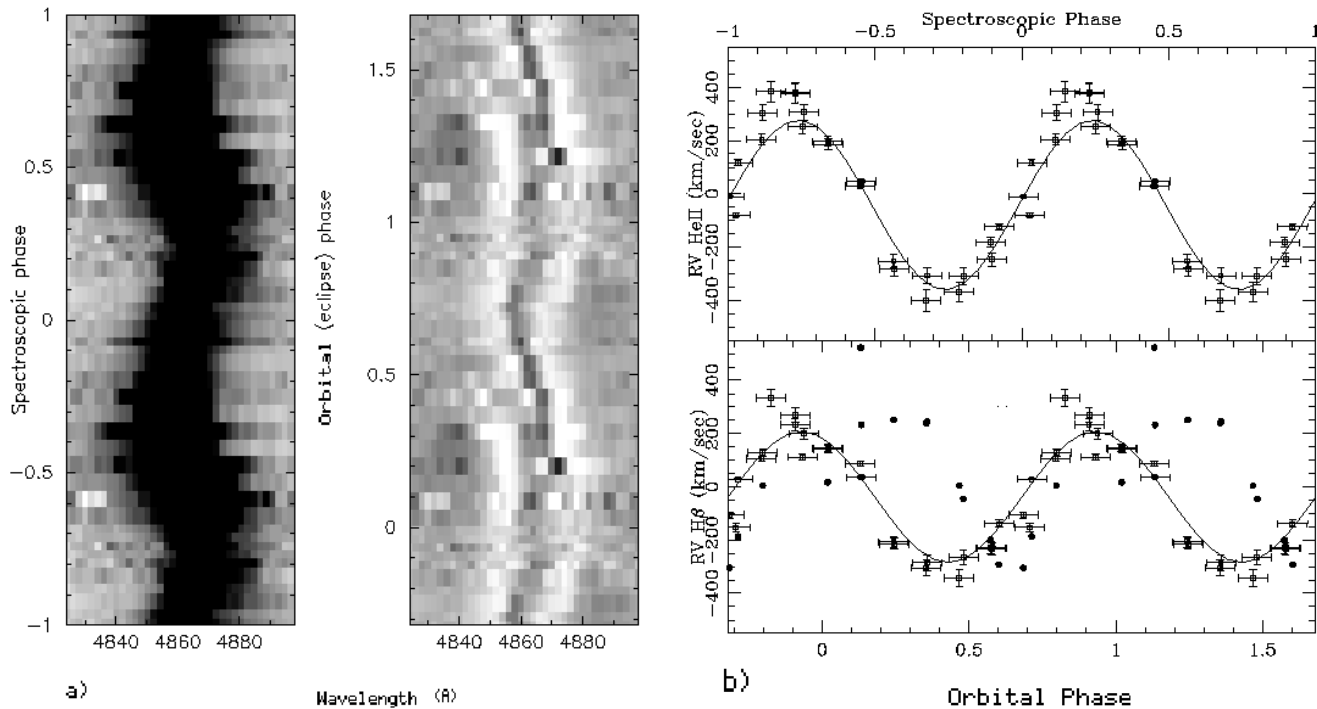


**Fig. 7. a)** The trailed spectra around  $H\beta$ . In the left panel the line wings are highlighted. In the right panel the same line is shown after subtraction of a gaussian fit with the center calculated from the spectroscopic phase. **b)** The radial velocity curves of He II (top) and  $H\beta$  (bottom). The error of measurements is marked by a vertical bar. The exposure length is marked by a horizontal bar. The solid circles in the lower panel indicate measurements of the emission feature as shown in the right panel of Fig. 7a.

or shortly before the shock, i.e. about 0.1 WD radii above the WD surface. The latter would be the more obvious location, but there we would expect much higher velocities, which we do not see.

### 3.7. The red and near-infrared spectrum

The near-infrared spectra reveal two strong emission features at  $\lambda$  8200 Å and  $\lambda$  8660 Å (Fig. 9). These coincide with the location of the Na I doublet and one of the components of the Ca II triplet. These lines could be recognised at some phases as absorption features seated on tremendously broad emission. In a huge sample of CVs observed by Friend et al. (1988), no object was found to display such a behaviour, although similar but much fainter features showed up in some accretion disc systems after subtraction of the secondary’s spectra. These features were referred to as “disc component” by Friend et al. (1990). In our case, however, these lines become prominent during eclipse and fade to halt at phase when we are looking along the accretion stream ( $\phi_{orb} = 0.7 - 0.85$ ).

At  $\lambda$  8204 Å happens to be the Paschen jump. Mukai and Charles (1987) have also observed excess emission at that wavelength in PG 1550+191, a well known polar. They argue that it could be due to the peak of the residual Paschen continuum (blend of discrete lines at the limit of

the Paschen series broadened by the Stark effect). However, they observed also lower series lines at significant strength, which is not the case for RX J0719.2+6557.

We also looked for possible absorption features in the red portion of the spectra, aimed in identifying the secondary star. The combined sensitivity of the spectrograph and CCD matrix drops rapidly redwards of  $\lambda$  7500 Å. Although we are able to see strong emission features and their changes, the continuum and absorption features are below  $S/N=10$  level, and are only marginally distinguished. Unfortunately, we have not observed any red dwarf standards simultaneously for comparison and cross-correlation.

We could not identify the strong TiO band features one would expect if we had a significant contribution of the secondary in the red part of the spectrum. Nevertheless, we found some hints witnessing a M 4–M 5.5 spectral type of the secondary. Young & Schneider (1981) and later Wade & Horne (1988) found quantitative spectral indices to estimate the spectral types of CV secondaries. Equivalent widths of the absorption features cannot be used directly in most cases, because they are affected by continuum from the WD+accretion structure, but flux deficits relative to a reference continuum remain unaffected. We followed roughly the procedure described by Wade & Horne (1988). First, we subtracted

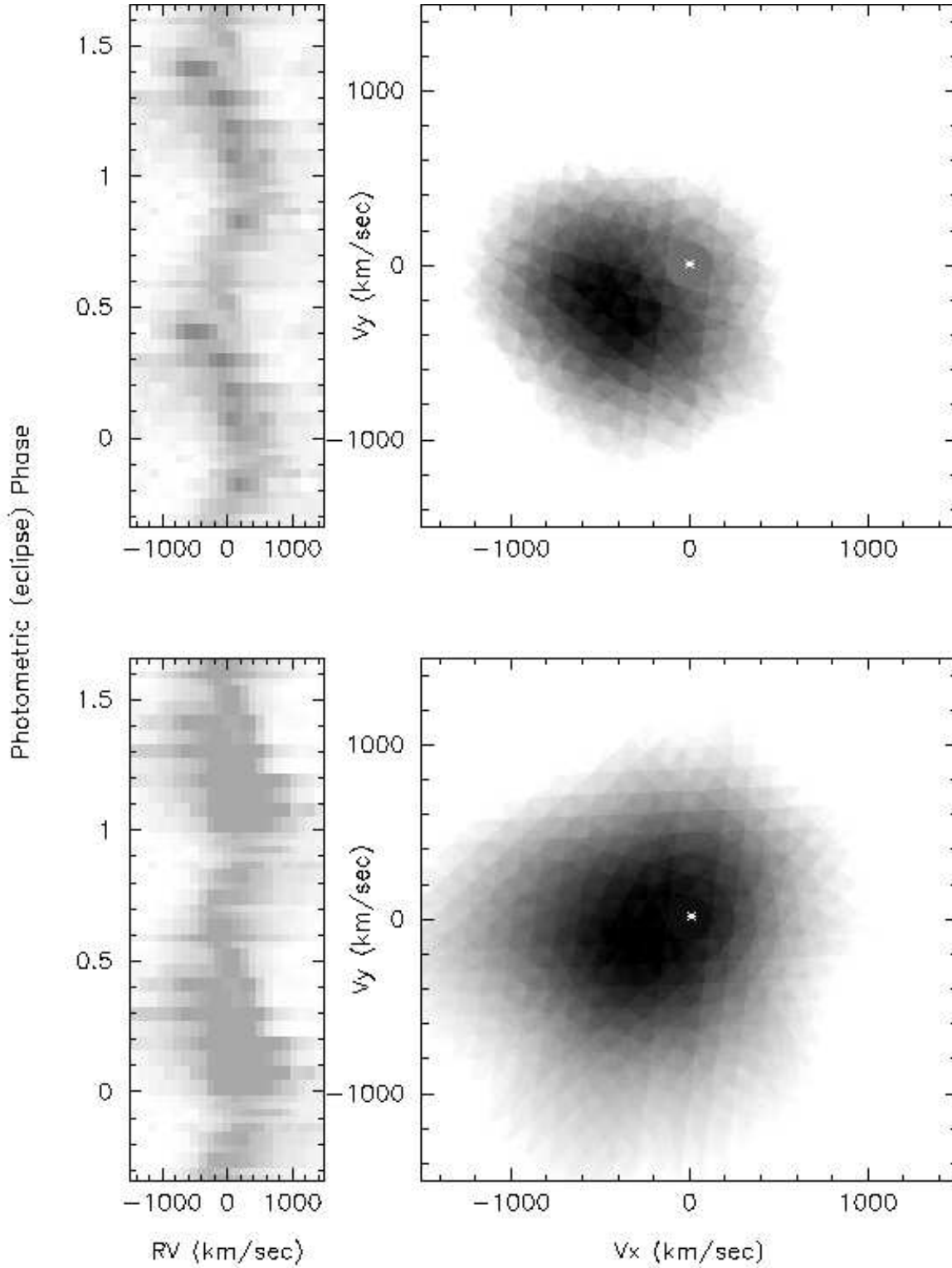


**Fig. 8.** The trailed spectra and images of the velocity plane of RX J0719.2+6557 of H $\beta$  (bottom) and He II (top) obtained by the backprojection method. The center of mass of the system is marked on the  $V_x - V_y$  images by a white symbol.



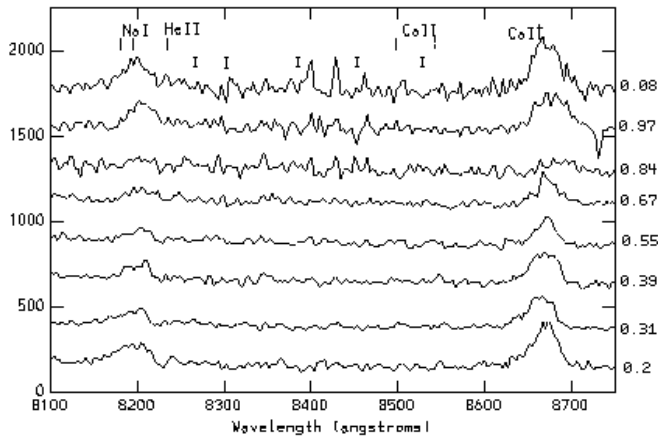


**Fig. 9.** The evolution of spectra in the spectral region between  $\lambda\lambda 7800 - 8900 \text{ \AA}$  through different orbital phases as marked on the right hand side. The numbers on the left side of the panel refer to the counts of the bottom spectrum. Other spectra are shifted up by 100% each. The spectral lines usually present in CV spectra are marked on the top. Vertical ticks mark some prominent TiO features in the spectra of M4–M6 red dwarfs.

the telluric line at  $\lambda 7600 \text{ \AA}$  by fitting each component by a gaussian using the outer wings on three spectra obtained in phases 0.9–0.1. Then we fitted the continuum to the spectra with a second order polynomial, which is almost a straight line in that part of the spectrum, and finally calculated the flux deficits of  $\lambda 7665 / \lambda 7165 \text{ \AA}$  of the TiO bands. The obtained values range between  $1.0 < d_\nu(\lambda 7665) / d_\nu(\lambda 7165) < 1.5$ , which corresponds to a M4–M6 spectral type. The accuracy of our measurements does not allow a more precise estimate. This is not surprising, because the majority of the short-period CVs below the period gap have late-type companions (Echevarría (1983), Tovmassian (1984)).

The absolute magnitude of a M5–6 main-sequence star (the non-illuminated side) ranges between  $M_V = 12.3\text{--}13.5$  mag. During the eclipse - when we see the back-side of the companion - the V brightness drops down to  $V \approx 19$  mag. This implies a lower limit for a distance of 100–150 pc, consistent with the rough guess from the X-ray absorption measure.

#### 4. Summary

The basic results of our observational study can be summarized as follows:

1. Based on the nature of the X-ray spectrum, the synchronized WD spin and orbital period, and despite the moderate strength of He II relative to  $H\beta$ , the ROSAT all-sky survey source RX J0719.2+6557 is identified as a new eclipsing polar. The orbital period is found to be 98.2 min. Narrow eclipses are observed which correspond to the occultation of the hot spot on the ac-

cretion stream by the companion. The eclipse period coincides with the radial velocity variations of the major emission lines.

2. The high amplitude of the radial velocity variations and its phasing relative to the eclipses allow us to conclude that the major line emission also comes from the frame of the accretion stream and hot spot. However, line emission requires different conditions (e.g. density) than continuum emission, so that the two emission regions are expected to be distinct. We were successful to retrieve also the weaker component of emission lines formed on the heated side of the secondary. The geometric interpretation fits well the usual picture of eclipsing polars in analogy with other similar magnetic cataclysmic variables.
3. From the absorption of the X-ray spectrum and the inferred absolute magnitude of the companion as compared to the observed one we estimate a lower limit of the distance to  $d \lesssim 100\text{--}150$  pc. The phase-averaged, unabsorbed X-ray luminosity is  $2.5 \times 10^{30} (D/100 \text{ pc})^2$  erg/s in the 0.1–2.4 keV range.
4. The Doppler tomography localizes the source of strong He II line emission to the accretion stream/hot spot. Other lines with lower excitation levels are more spread out over the system.
5. The detection of the two emission lines at  $8200 \text{ \AA}$  and  $8660 \text{ \AA}$  is one of the most exciting (and barely understood) results of these observations. Although we were unable to identify them with any known lines, their presence implies the existence of conditions in RX J0719.2+6557 which arise in very few systems only (based on the lack of detections in many other polars). Unfortunately, the amount of existing data does not yet allow any further conclusions.
6. A low magnetic field for the white dwarf is suggested by three facts: (a) The optical spectrum does not show hints for cyclotron lines. (b) The X-ray spectrum is observed to be rather hard. The soft-to-hard X-ray flux ratio for polars with measured magnetic field strengths has been shown to increase with magnetic field (Beuermann & Schwöpe 1994). (c) The stronger photometric modulation in red than in blue and its phasing also argues for a low magnetic field.

*Acknowledgements.* GT thanks Allen Shafter for discussing details of the reduction technique and providing parts of the analysis code. The authors are grateful to R. Schwarz and to the referee M. Mouchet for valuable comments and discussions which considerably improved the presentation of our results. This work was partially financed by the DGAPA project IN109195. JG is supported by the Deutsche Agentur für Raumfahrtangelegenheiten (DARA) GmbH under contract FKZ 50 OR 9201 and 50 QQ 9602 3. The ROSAT project is supported by the German Bundesministerium für Bildung, Wissenschaft, Forschung und Technologie (BMBF/DARA) and the Max-Planck-Society.

## References

- Beuermann K., Schwobe A.D., 1994, in *Interacting Binary Stars*, ed. A.W. Shafter, ASP Conf. Series 56, p. 119
- Dickey J.M., Lockman F.J., 1990, *Ann. Rev. Astron. Astrophys.* 28, 215
- Echevarría J., 1983, *Rev. Mex. Astron. Astrofis* 8, 109
- Friend M.T., Martin J.S., Smith R.C., Jones D.H.P., 1988, *MNRAS* 233, 451
- Friend M.T., Martin J.S., Smith R.C., Jones D.H.P., 1990, *MNRAS* 246, 637
- Horne K., 1986, *PASP* 98, 609
- Marsh T.R., Horne K., 1988, *MNRAS* 235, 269
- Mukai K., Charles P.A., 1987, *MNRAS* 226, 209
- Schneider D.P., Young P., 1980, *ApJ* 238, 946
- Shafter A.W., 1985, in *Cataclysmic Variables and Low Mass X-ray Binaries*, eds. D.Q. Lamb and J. Patterson (Dordrecht: D. Reidel Pub. Co.) p. 355
- Tovmassian G.H., 1984, *Afz* 21, 289
- Tovmassian G., Greiner J., Zickgraf F.-J., Kroll P., Krautter J., Thiering I., Serrano A., 1997, in *Accretion Phenomena and Associated Outflows*, Proc. of IAU Coll. 163 (in press) (astro-ph/9609166)
- Wade R.A., Horne K., 1988, *ApJ* 324, 411
- Warner B., 1995, Proc. Cape Workshop on Magnetic CVs, ASP Conf. Ser. 85, 3
- Young P., Schneider D.P., 1981, *ApJ* 247, 960
- Zickgraf F.-J., Thiering I., Krautter J., Appenzeller I., Kneer R., Voges W., Ziegler B., Chavarria, C., Serrano A., Mujica R., Pakull M., Heidt J., 1997, *A&AS* (in press)